European Polymer Journal 175 (2022) 111342

Contents lists available at ScienceDirect

European Polymer Journal

journal homepage: www.elsevier.com/locate/europolj

Synthesis and anisotropic growth of glycerol-based thermoresponsive NIR plasmonic nanogels

Emanuel A. Glitscher [a,1], Julian Bergueiro [a,b,1], Marcelo Calderón [a,c,d,*]

[a] Freie Universität Berlin, Institute for Chemistry and Biochemistry, Takustrasse 3, 14195 Berlin, Germany
[b] Centro Singular de Investigación en Química Biolóxica e Materiais Moleculares (CIQUS), Departamento de Química Orgánica, Universidade de Santiago de Compostela, 15782 Santiago de Compostela, Spain
[c] POLYMAT, Applied Chemistry Department, Faculty of Chemistry, University of the Basque Country UPV/EHU, Paseo Manuel de Lardizabal 3, 20018 Donostia-San Sebastián, Spain
[d] IKERBASQUE, Basque Foundation for Science, 48009 Bilbao, Spain

ARTICLE INFO

Keywords:
Nanogels
Thermoresponsive
Gold nanoparticles
Photothermal agent
Cancer therapy
Nanocarrier
Drug delivery

ABSTRACT

Polymeric thermoresponsive nanogels (NGs) have shown their potential in the field of nanomedicine. Providing their structure with additional smart modalities to broaden their application scope remains challenging. We hereby describe a novel and convenient strategy for NGs' construction with anisotropic gold nanoparticles (AuNPs) incorporated. AuNPs act as both, crosslinking points, and light to heat transducers. In our strategy, we incorporate small plasmonic AuNPs that are further anisotropically grown conferring the nanogel with NIR responsive capabilities.

1. Introduction

Nanogels (NGs) are relatively young materials with high application potential. NGs are considered among other nanomaterials for the transport and controlled release of therapeutic and diagnostic cargos and therefore, for the treatment of diseases like cancer [1,2]. NGs combine chemical stability, high biocompatibility, water solubility, and high swelling and loading capacity for encapsulation of molecules [3]. Swelling behaviour of NGs depends on their building blocks chemical composition and the density of the polymeric network [4].

NGs can selectively release their cargo upon changes in the environment [5]. The use of polymeric materials with lower critical solution temperatures (LCST) emerged in the last years [6,7]. Especially LCST-polymers based on glycidyl ether monomers show high biocompatibility and sharp phase transitions tuneable in physiological relevant temperature ranges by simply controlling the polymer length and monomer ratio [8].

On the other hand, the incorporation of suitable phototransducers into NGs can trigger the phase transition upon mild non-invasive irradiation without applying external heat [9]. In particular, near infra-red (NIR) light is suitable for most targeted biological applications since it is able to penetrate deeply into any tissue [10]. Thus, phototransducers that can convert NIR light into heat represent a perfect synergy with the thermoresponsive NGs for the abovementioned applications. Inorganic materials are frequently used as phototransducers in theranostic applications as they do not suffer from drawbacks like low absorption coefficients or photo-bleaching [11,12]. Particularly, gold nanoparticles (AuNPs) show superior photothermal conversion efficiencies due to localized surface plasmon resonance (LSPR) and have been widely considered for imaging [13], drug delivery [14], and photothermal therapy [15]. However, to tune the absorbance of the AuNPs to the NIR region it is required to use anisotropic gold shapes, that have a big dimensions and need to be previously synthesized with relative complex methodologies. The particle dimensions complicate their inclusion in porous materials like nanogels and present insufficient excretion and long-term accumulation in organs after application [16].

Herein, we report the synthesis of thermoresponsive gold nanogels (AuNGs) based on poly(glycidyl ether) and cross-linked by small alkyne-functionalized AuNPs via click chemistry and thermo-nanoprecipitation (TNP) and their further anisotropic growth of the spherical AuNPs inside the nanogels. The resulting NIR-absorbing thermoresponsive gold nanogels (NIRAuNGs) show high NIR light to heat conversion efficiency.

* Corresponding author.
E-mail address: marcelo.calderon@polymat.eu (M. Calderón).
[1] These authors contributed equally.

https://doi.org/10.1016/j.eurpolymj.2022.111342
Received 13 April 2022; Received in revised form 31 May 2022; Accepted 6 June 2022
Available online 9 June 2022

2. Results and discussion

AuNGs were synthesized by cross-linking of thermoresponsive poly (glycidyl methyl ether-co-ethyl glycidyl ether) (tPG) with alkyne-functionalized AuNPs. tPG was synthesized by anionic ring opening polymerization of the monomers glycidyl methyl ether (GME) and ethyl glycidyl ether (EGE) in 1:1 feed ratio according to literature (Fig. 1A, Left, Figure S1) [17]. Co-polymers with this ratio and a molecular weight of 5 kDa develop phase transition in physiological relevant temperature ranges [18]. The resulting polymer was further converted into bi-azide-functionalized N_3-tPG-N_3 by mesylation of the terminal alkoxy group and subsequent azidation of both functional end groups. The cloud point temperature (T_{cp}) was determined to be of 33.5 °C for 1 wt% solutions [19].

As second building block, small spherical AuNPs with diameters ranging from 2 to 5 nm are most suitable for the internalization in NGs as they show comparable sizes to other polymeric macromolecular cross-linkers already used for the synthesis of NGs [20]. Thus, 11-mercaptoundecanoic propargylamide (MUPA), synthesized by amide coupling of 11–mercaptoundecanoic acid (MUA) and propargyl amine, was used as alkyne functionalized ligand in the AuNPs. The functionalization of alkyne decorated AuNPs was performed in a two-phase liquid–liquid approach accordingly to established procedures (Fig. 1A, Right, Figure S1) [21]. To acquire control over the functionalization and the number of cross-linking points, a combination of MUPA and MUA was used. The carboxylic acid units introduced by MUA also increase hydrophilicity of the AuNPs which is favourable for targeted in vivo applications and additionally prevents the particles from aggregation in aqueous solution. Elemental analysis of carbon, hydrogen, nitrogen, and sulphur gave organic/inorganic weight ratio from which the composition of AuNP@MUPA/MUA can be deduced. The particles consist of 70% inorganic and 30% organic material which is in good agreement with reports of AuNPs with comparable size and ligands [21]. The alkyne functionalization degree (35%) was determined by ^{1}H NMR and used together with elemental analysis to calculate the molar amount of alkyne units per weight (Figure S2–7). Statistical analysis of the size distribution shows a mean diameter of 2.6 ± 1.6 nm analysed by transmission electron microscopy (TEM) (Figure S8).

For the synthesis of the thermoresponsive AuNGs, we applied a novel TNP protocol for the formation of poly(glycidyl ether) based NGs (Fig. 1A, Center) [19]. This method is suitable for the formation of nanometer-sized polymeric particles with narrow size distributions and precise control over their thermoresponsive properties. AuNP@MUPA/MUA and tPG-N_3 were solubilized and mixed in dimethylformamide (DMF) to induce cross-coupling by copper-promoted azide alkyne cycloaddition (CuAAC) and then precipitated in water above the transition temperature of the thermoresponsive polymer (45 °C). Pre-mixing of the components for at least 6 h was necessary to assure sufficient coupling for a good nucleation. We assume that the copper ions not only interact with the alkyne units, but also with the carboxylic acids which would explain the slow reaction rate [22]. We applied a rational screening of the reactant and solvent/non-solvent ratios to yield particles with optimal sizes and monodispersity. K_2CO_3 was added to increase the solubility and prevent aggregation of AuNP@MUPA/MUA by deprotonation of the carboxylic acid groups. Unreacted building blocks and copper salts were removed by dialysis and centrifugation (See ESI for details).

To achieve control over the AuNG size for targeting biological applications, the ratio of building blocks in the TNP was screened (Table S1). The amount of AuNP@MUPA/MUA was varied with respect to tPG and sizes were evaluated by dynamic light scattering (DLS) and nanoparticle tracking analysis (NTA). The resulting mean diameters showed a significant tendency when varying the amount of AuNP cross-linkers. Narrow size distributions were reached for AuNGs synthesized with 80 wt% AuNPs (ratio azide/alkyne: 1:0.8). The mean hydrodynamic diameter (d) measured by DLS was 87.5 nm (PDI = 0.16), whereas NTA showed a similar mean size of 94.9 nm (SD 58.5 nm) (Fig. 2B). Increasing the cross-linking points with a higher AuNPs ratio to polymer (160 to 320 wt% AuNPs) resulted in AuNGs with increased d between 133 and 187 nm. More significantly, the PDI increased drastically up to more than 0.4 for AuNGs synthesized under certain conditions which is illustrated by polydisperse size distributions (Figure S9). Still, TNP shows high reproducibility under the given optimal conditions and the resulting AuNGs were stable in aqueous solution at 4 °C for at least twelve months which is favourable compared to systems based on other more rapidly oxidizing metal particles [23].

Further characterization was achieved by absorption and transmittance UV–Vis spectroscopy for AuNGs synthesized with 80 wt% AuNPs, as these nanogels showed optimal results in terms of their size and PDI for biological applications. The absorption profile of the AuNGs shifted slightly to higher wavelengths (570 nm) in contrast to AuNP@MUPA/MUA (520 nm), assumingly because of plasmon coupling between adjacent AuNPs (Figure S10) [24]. Temperature-sensitivity of AuNGs was validated by transmittance of light against temperature (Fig. 1C). T_{cp} values were measured for all synthesized NGs. Sharp transitions of AuNGs were detected between 34.5 and 36.6 °C with a minor tendency for higher temperatures when increasing the amount of cross-linkers during synthesis (Table S1). AuNGs with 80 wt% cross-linker amount exhibit T_{cp} at 35.3 °C for 1 mg/mL and 45.2 °C for 0.1 mg/mL aqueous solutions. Lower concentrations are a good

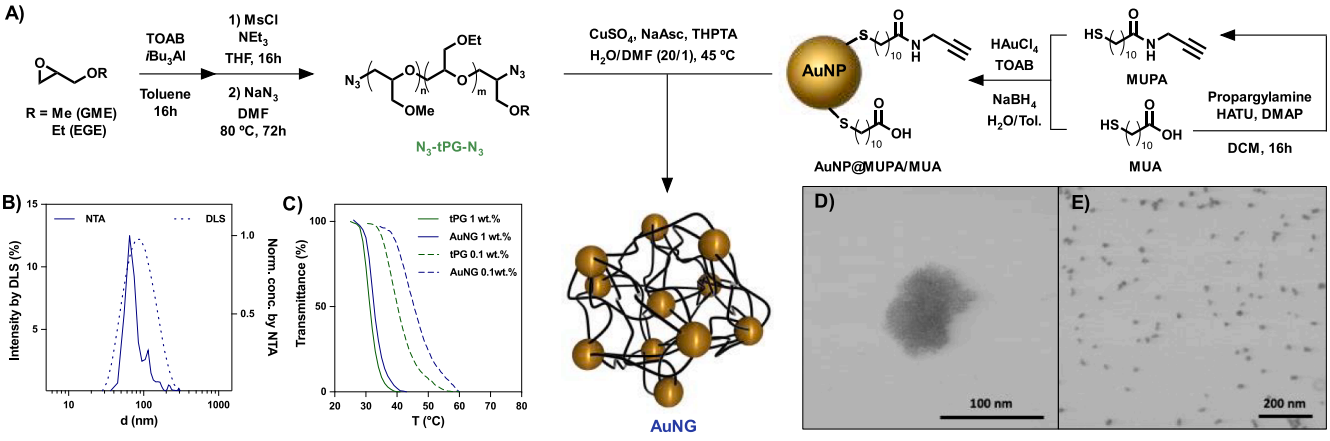

Fig. 1. (A) Left: Synthesis of tPG by anionic ring opening polymerization and conversion of both functional end groups to azide moieties. Middle: Synthesis of AuNGs by CuAAC and TNP. Right: Synthesis of AuNP@MUPA/MUA. (B) Size distributions by intensity (DLS) and particle count (NTA) of AuNGs in neutral aqueous solution. (C) Phase transition of tPG and AuNGs measured by transmittance of light at 700 nm against the temperature. (D-E) TEM images of AuNGs with 80 wt% AuNPs feed.

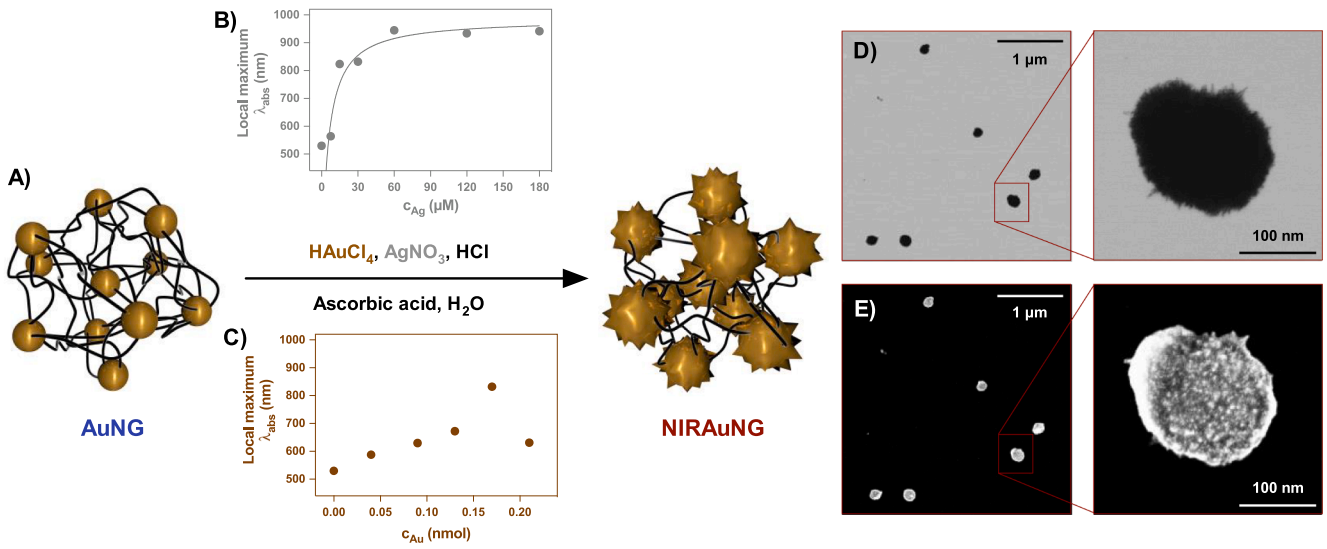

Fig. 2. (A) Anisotropic growth of the AuNPs inside the polymeric NG(NaAsc, sodium ascorbate; THPTA, tris(3-hydroxypropyltriazolyl-methyl)amine). (B) Au^{3+} and (C) Ag^{+} ions concentration effect on the anisotropic growth of the AuNGs. For screening gold, the silver concentration was kept constant at 30 μM, for screening silver, the gold concentration was kept constant at 180 μM. (D) TEM (E) SEM images of NIRAuNGs. (F) Size distribution by particle count (NTA) of NIRAuNGs compared to AuNGs in neutral aqueous solution. (G) Phase transition of NIRAuNGs and AuNGs measured by transmittance of light at 700 nm against the temperature for 0.25 wt% aqueous solution. (H) Photothermal conversion curves of NIRAuNGs at different concentrations irradiated with a 785 nm laser. Data shown mean and SD of three measurements. Ungrown AuNGs were measured at 0.5 mg/mL (blue line), water serves as negative control (black line). Irradiation was always started at room temperature (25 °C). (For interpretation of the references to colour in this figure legend, the reader is referred to the web version of this article.)

reference for the in vivo scenario in which the transition temperature of the system is above the nanogel T_{cp}. Such range and appearance of the phase transition is in good agreement to other reported tPG based NGs [19,25]. The phase transition curve shows minor broadening at 0.1 mg/mL due to less NG-NG interactions at lower concentrations. For all AuNGs, the diameter by DLS reached values between 242 and 291 nm when measured at 45 °C indicating aggregation of the nanogels above the volume-phase transition temperature (VPTT). Determining the VPTT itself by temperature-dependant DLS measurement shows identical temperature ranges for the transition as for the T_{cp} at 1 mg/mL (Figure S11). Deduced from both techniques, incorporated AuNPs show a neglectable influence on the hydrophilicity and the phase transition behaviour of the polymeric material and the NGs.

TEM and scanning electron microscopy (SEM) images were obtained to additionally visualize the arrangement of highly cross-linked AuNGs. Images show compact and dense NGs particles with diameters between 40 and 60 nm (Fig. 1D-E). AuNGs are reduced approximately half in diameter compared to DLS measurements since the particles shrink when dried for TEM preparation under high vacuum. TEM was additionally used to investigate the effect that the cross-linker amount has on the general appearance of the NGs. Images of AuNGs prepared with higher amounts of cross-linking AuNPs present larger and denser nanogels with diameters up to 100–200 nm. Assumingly, increasing the amount of cross-linkers leads to an increased size of NGs due to lower number of polymer chains per gold particle whereas fewer cross-linkers induce the formation of less compact and more chain-like structures with high polydispersity (Figure S12).

Anisotropic growth of AuNPs bathochomically shifts the plasmon absorbance to the NIR region [26]. However, the controlled and selective growth of AuNPs inside polymeric material is still underrepresented due to the inherent complexity of the process. Conveniently, NGs can easily swell and incorporate in their interior the salts and reductants necessary for the anisotropic growth [27]. We took advantage of this fact to grow anisotropic structures from AuNPs embedded inside polymeric nanogels and thus red-shift the absorption profile to the NIR region. For the synthesis of NIRAuNGs, we employed surfactant-free growing conditions with tetrachloroauric acid and silver nitrate as shape determining agent, and ascorbic acid as reductant.

For a uniform growth, first the AuNGs were incubated with $HAuCl_4$, followed by simultaneous addition of $AgNO_3$ and ascorbic acid (Fig. 2A). Ultrasonication was necessary to guarantee homogenous distribution of the growing components inside the nanogel volume and showed optimal results for the growing. According to the rapid colour change, the initial growth of AuNPs inside the nanogels proceeded within seconds. The growth process was monitored by UV–Vis spectroscopy and halted after approximately 15 min, as no further significant alteration of the absorption profile was observed. The process was stopped by centrifugation and redispersion in water.

As expected, the change in absorption profiles is highly sensitive to the reaction conditions and depends on the amount and ratio of gold and silver ions used as well as temperature and pH (Table S2). Small amounts of HCl are crucial for the growth of anisotropic structures. Without HCl in the growing solution, the maximum absorption remained below 600 nm. Under low concentrations of H^{+} ions, the dissociation of ascorbic acid proceeds fast resulting in immediate reduction of a high amount of gold ions. This leads to an instant formation of a high number of nuclei and spherical growth of the particles [28]. Slower dissociation of ascorbic acid at acidic pH results in an anisotropic growth directed by the additional silver ions. The same tendency occurred, when performing the growth at 45 °C (Figure S13) since the AuNGs are collapsed at this temperature and not able to internalize the reactives. All growing experiments were performed in an ultrasonic bath set to 25 °C and the amount of AuNGs as seed particles was fixed in all cases at 25 μg/mL.

Different ratios of the reactants were examined to tune the absorbance to the NIR region. Screening of the silver amount led to a strong red-shift of absorbance when increasing concentration (Fig. 2B). The local λ_{max} shifted to 750 nm for 15 mM silver and further to 970 nm for 60 mM silver but remained around 960 nm under even higher silver concentrations. A similar behaviour can be observed for the growth of gold nanostars, where higher amounts of silver lead to an increased number of spikes and plasmon band red-shifting [27]. For other AuNPs like rods and prisms, the silver concentration determines the aspect ratio having as well a strong effect on the plasmon resonance band [29]. When altering the gold salt concentration, signal broadening occurred without λ_{max} shifting above 600 nm for low amounts of gold (Fig. 2C). Gold concentration has not a pronounced influence on the shape. Low

amounts lead to an incomplete growth whereas high amounts can lead to an overgrowth on all particle facets, giving larger spherical particles. Ideal NIRAuNGs growth conditions were reached as followed: Optimal concentrations in the reaction solution were adjusted as for 30 μM for $AgNO_3$ and 170 μM for $HAuCl_4$. NIRAuNGs grown under these conditions exhibit a λ_{max} at 870 nm and did not exhibit fast aggregation as observed for NIRAuNGs grown with higher amounts of silver.

Under these specific conditions, optimal results concerning size, absorption profile, and appearance were achieved. AuNPs exhibit structural growing at the outer and inner parts of the nanogels, as evidenced with SEM (Fig. 2E). NIRAuNGs nevertheless retained their spherical shape and compact structure exhibiting sizes from 150 to 180 nm in TEM/SEM. The spiky nature of the newly grown gold nanostructures inside the gels explains both broadening and plasmon red-shifting.

NIRAuNGs grown under other conditions experienced non-uniform growth. TEM/SEM images reveal the formation of large prismatic nanoparticles in the nanogels when using high amounts of silver. Similar observations in TEM/SEM were made when changing the amount of gold salt in the growing solution. Here, the AuNPs inside the NGs itself exhibit bigger sizes, less anisotropic growth, and higher polydispersity as the absorption did not significantly red-shifted when altering the gold concentrations (Figure S14). We conclude that the ratio between gold and silver ions (optimal conditions, Au:Ag 5.7:1) as well as the total amount of metal ions in the growing solution (Au 0.17 mM, Ag 30 μM) is crucial for a uniform structural growth of the AuNPs inside the NGs and for the exhibition red-shift in absorbance. The high sensitivity of the anisotropic growth to the slightest changes in ratio of reactants is reported for a whole variety of different shapes and is reflected here as well [30].

NIRAuNGs grown under optimal conditions developed best characteristics concerning absorption profile and uniform growth of incorporated AuNPs. Mean size of 152.2 nm (SD 78.7 nm) was measured by NTA (Fig. 3A). NIRAuNGs still showed a sharp reversible phase transition at 39.4 °C measured at 0.25 mg/mL (Fig. 3B). Potentially, the increased amount of gold inside the NGs slightly shifts the T_{cp} towards lower values compared to the ungrown AuNGs as the additional gold surface increases the hydrophobicity of the system. Consideration for using the system as drug delivery agents is supported by detecting the T_{cp} above body temperature at this concentration. Applied in vivo, the NGs would still remain in soluble state if not heated above the transition temperature which could be achieved by irradiation of the NIRAuNGs with NIR light.

To validate sufficient NIR light-to-heat conversion, samples with different concentrations in aqueous solution were irradiated continuously with a 785 nm laser at a power density of 0.59 W/cm^2 for 5 min and the temperature was monitored by a thermal camera. NIRAuNGs showed a concentration dependent increment in temperature (ΔT) as screened in concentrations from 0.25 to 1 mg/mL (Fig. 3C). The temperature curves reached a stable plateau after approximately 90 s and show preservation of the maximum temperature for another three and a half minutes. At the highest measured concentration of 1 mg/mL, temperatures of 69 °C (ΔT = 44 °C) were reached. Lowering the concentration to 0.5 and 0.25 mg/mL showed maximum temperatures at 55 °C

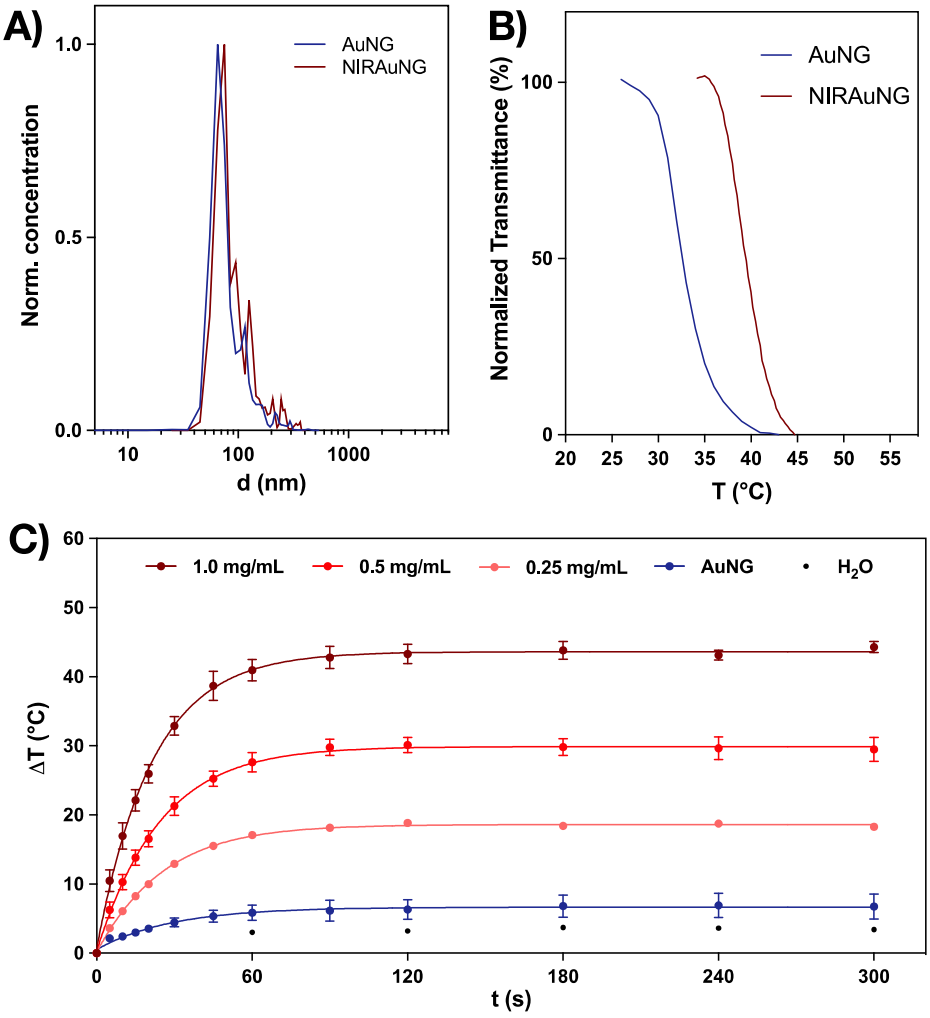

Fig. 3. (A) Size distribution by particle count (NTA) of NIRAuNGs compared to AuNGs in neutral aqueous solution. (B) Phase transition of NIRAuNGs and AuNGs measured by transmittance of light at 700 nm against the temperature for 0.25 wt% aqueous solution. (C) Photothermal conversion curves of NIRAuNGs at different concentrations irradiated with a 785 nm laser. Data shown mean and SD of three measurements. Ungrown AuNGs were measured at 0.5 mg/mL (blue line), water serves as negative control (black line). Irradiation was always started at room temperature (25 °C). (For interpretation of the references to colour in this figure legend, the reader is referred to the web version of this article.)

(ΔT = 30 °C) and 44 °C (ΔT = 19 °C) respectively. Under all three tested concentrations, temperatures above the T_{cp} of the nanogels were reached. In contrast to that, not grown AuNGs only exhibit an increment of 6 °C measured at 0.5 mg/mL, whereas water as a negative control showed no significant rise in temperature under NIR irradiation. The photothermal conversion efficiency of AuNGs was calculated to 34% with a concentration of 0.25 mg/mL [31]. This value is comparable with other reported anisotropic plasmonic systems designed for photothermal therapies [32,33]. The photothermal conversion properties of NIRAuNGs are therefore sufficient in terms of rising the temperature above the transition temperature of the NGs.

3. Conclusion

We presented the synthesis and characterization of tPG-based AuNGs, where AuNPs were introduced as cross-linkers for the polymeric chains. The nanogel particles showed convenient sizes below 100 nm with narrow size distributions, high stability in water, and reversible temperature-dependant phase transition in the range of 34 to 37 °C. Incorporated AuNPs were anisotropically reshaped inside the nanogel by precisely tuning the growing parameters. Hence, the absorbance maximum was shifted successfully to the NIR region. Proven by NTA and TEM, original size, and spherical shape of the nanogels were retained. With this change in plasmon absorbance, NIRAuNGs are able to convert NIR light into heat which we showed by short-time irradiation with a 785 nm laser. The temperature of the surrounding medium was raised above the VPTT of the nanogels even at low concentrations such as 0.25 mg/mL. NIRAuNGs will be utilized for future in vivo and in vitro photothermal therapy studies.

CRediT authorship contribution statement

Emanuel A. Glitscher: Data curation, Formal analysis, Investigation, Methodology, Writing – original draft. **Julian Bergueiro:** Data curation, Formal analysis, Investigation, Methodology, Writing – original draft, Writing – review & editing. **Marcelo Calderón:** Conceptualization, Data curation, Formal analysis, Funding acquisition, Project administration, Resources, Supervision, Writing – review & editing.

Declaration of Competing Interest

The authors declare that they have no known competing financial interests or personal relationships that could have appeared to influence the work reported in this paper.

Acknowledgements

We gratefully acknowledge financial support from the Bundesministerium für Bildung und Forschung (BMBF) through the NanoMatFutur award (13N12561, Thermonanogele). We would like to acknowledge the assistance of the Core Facility BioSupraMol supported by the Deutsche Forschungsgemeinschaft (DFG). EG and JB contributed equally to this work.

Data availability

The raw/processed data required to reproduce these findings cannot be shared at this time due to technical or time limitations.

Appendix A. Supplementary material

Supplementary data to this article can be found online at https://doi.org/10.1016/j.eurpolymj.2022.111342.

References

[1] M. Molina, M. Asadian-Birjand, J. Balach, J. Bergueiro, E. Miceli, M. Calderón, Stimuli-responsive nanogel composites and their application in nanomedicine, Chem. Soc. Rev. 44 (17) (2015) 6161–6186, https://doi.org/10.1039/c5cs00199d.
[2] H.-Q. Wu, C.-C. Wang, Biodegradable smart nanogels: a new platform for targeting drug delivery and biomedical diagnostics, Langmuir 32 (25) (2016) 6211–6225, https://doi.org/10.1021/acs.langmuir.6b00842.
[3] J.C. Cuggino, E.R.O. Blanco, L.M. Gugliotta, C.I.A. Igarzabal, M. Calderón, Crossing biological barriers with nanogels to improve drug delivery performance, J. Control. Release. 307 (2019) 221–246, https://doi.org/10.1016/j.jconrel.2019.06.005.
[4] X. Zhang, S. Malhotra, M. Molina, R. Haag, Micro- and nanogels with labile crosslinks – from synthesis to biomedical applications, Chem. Soc. Rev. 44 (7) (2015) 1948–1973, https://doi.org/10.1039/c4cs00341a.
[5] E. Fleige, M.A. Quadir, R. Haag, Stimuli-responsive polymeric nanocarriers for the controlled transport of active compounds: Concepts and applications, Adv. Drug. Deliver. Rev. 64 (9) (2012) 866–884, https://doi.org/10.1016/j.addr.2012.01.020.
[6] J. Bergueiro, M. Calderón, Thermoresponsive nanodevices in biomedical applications, Macromol. Biosci. 15 (2) (2015) 183–199, https://doi.org/10.1002/mabi.201400362.
[7] M.I. Gibson, R.K. O'Reilly, To aggregate, or not to aggregate? considerations in the design and application of polymeric thermally-responsive nanoparticles, Chem. Soc. Rev. 42 (17) (2013) 7204–7213, https://doi.org/10.1039/c3cs60035a.
[8] M. Weinhart, T. Becherer, R. Haag, Switchable, biocompatible surfaces based on glycerol copolymers, Chem. Commun. 47 (5) (2011) 1553–1555, https://doi.org/10.1039/c0cc04002a.
[9] C. Biglione, J. Bergueiro, S. Wedepohl, B. Klemke, M.C. Strumia, M. Calderón, Revealing the NIR-triggered chemotherapy therapeutic window of magnetic and thermoresponsive nanogels, Nanoscale 12 (42) (2020) 21635–21646, https://doi.org/10.1039/d0nr02953j.
[10] Y. Yang, J. Aw, B. Xing, Nanostructures for NIR light-controlled therapies, Nanoscale 9 (11) (2017) 3698–3718, https://doi.org/10.1039/c6nr09177f.
[11] X. Yang, M. Yang, B.o. Pang, M. Vara, Y. Xia, Gold nanomaterials at work in biomedicine, Chem. Rev. 115 (19) (2015) 10410–10488, https://doi.org/10.1021/acs.chemrev.5b00193.
[12] E.C. Dreaden, A.M. Alkilany, X. Huang, C.J. Murphy, M.A. El-Sayed, The golden age: gold nanoparticles for biomedicine, Chem. Soc. Rev. 41 (7) (2012) 2740–2779, https://doi.org/10.1039/c1cs15237h.
[13] S. Liang, C. Li, C. Zhang, Y. Chen, L. Xu, C. Bao, X. Wang, G. liu, F. zhang, D. Cui, CD44v6 monoclonal antibody-conjugated gold nanostars for targeted photoacoustic imaging and plasmonic photothermal therapy of gastric cancer stem-like cells, Theranostics. 5 (9) (2015) 970–984, https://doi.org/10.7150/thno.11632.
[14] L. Jing, X. Liang, X. Li, L.i. Lin, Y. Yang, X. Yue, Z. Dai, Mn-porphyrin conjugated Au nanoshells encapsulating doxorubicin for potential magnetic resonance imaging and light triggered synergistic therapy of cancer, Theranostics 4 (9) (2014) 858–871, https://doi.org/10.7150/thno.8818.
[15] T. Patino, U. Mahajan, R. Palankar, N. Medvedev, J. Walowski, M. Münzenberg, J. Mayerle, M. Delcea, Multifunctional gold nanorods for selective plasmonic photothermal therapy in pancreatic cancer cells using ultra-short pulse near-infrared laser irradiation, Nanoscale 7 (12) (2015) 5328–5337, https://doi.org/10.1039/c5nr00114e.
[16] N. Khlebtsov, L. Dykman, Biodistribution and toxicity of engineered gold nanoparticles : a review of in vitro and in vivo studies, Chem. Soc. Rev. 40 (2010) 1647–1671, https://doi.org/10.1039/c0cs00018c.
[17] A. Labbé, S. Carlotti, C. Billouard, P. Desbois, A. Deffieux, controlled high-speed anionic polymerization of propylene oxide initiated by onium salts in the presence of triisobutylaluminum, Macromolecules 40 (22) (2007) 7842–7847, https://doi.org/10.1021/ma070288d.
[18] S. Heinen, S. Rackow, A. Schäfer, M. Weinhart, A perfect match: fast and truly random copolymerization of glycidyl ether monomers to thermoresponsive copolymers, Macromolecules 50 (1) (2017) 44–53, https://doi.org/10.1021/acs.macromol.6b01904.
[19] M. Giulbudagian, M. Asadian-Birjand, D. Steinhilber, K. Achazi, M. Molina, M. Calderón, Fabrication of thermoresponsive nanogels by thermo-nanoprecipitation and in situ encapsulation of bioactives, Polym. Chem-Uk. 5 (24) (2014) 6909–6913, https://doi.org/10.1039/c4py01186d.
[20] J.C. Cuggino, C.I. Alvarez I., M.C. Strumia, P. Welker, K. Licha, D. Steinhilber, R.-C. Mutihac, M. Calderón, Thermosensitive nanogels based on dendritic polyglycerol and N-isopropylacrylamide for biomedical applications, Soft. Matter. 7 (23) (2011) 11259, https://doi.org/10.1039/c1sm06357j.
[21] M. Brust, M. Walker, D. Bethell, D.J. Schiffrin, R. Whyman, Synthesis of thiol-derivatised gold nanoparticles in a two-phase Liquid-Liquid system, J. Chem. Soc. Chem. Commun. 0 (7) (1994) 801–802, https://doi.org/10.1039/c39940000801.
[22] T. Bala, B.L.V. Prasad, M. Sastry, M.U. Kahaly, U.V. Waghmare, Interaction of different metal ions with carboxylic acid group: a quantitative study, J. Phys. Chem. 111 (2007) 6183–6190, https://doi.org/10.1021/jp067906x.
[23] K.S. Siddiqi, A. Husen, R.A.K. Rao, A review on biosynthesis of silver nanoparticles and their biocidal properties, J. Nanobiotechnol. 16 (2018) 14, https://doi.org/10.1186/s12951-018-0334-5.
[24] P.K. Jain, M.A. El-Sayed, Plasmonic coupling in noble metal nanostructures, Chem. Phys. Lett. 487 (4-6) (2010) 153–164, https://doi.org/10.1016/j.cplett.2010.01.062.
[25] M. Asadian-Birjand, C. Biglione, J. Bergueiro, A. Cappelletti, C. Rahane, G. Chate, J. Khandare, B. Klemke, M.C. Strumia, M. Calderón, Transferrin decorated thermoresponsive nanogels as magnetic trap devices for circulating tumor cells,

Macromol. Rapid Comm. 37 (5) (2016) 439–445, https://doi.org/10.1002/marc.201500590.
[26] Y. Lu, J. Yuan, F. Polzer, M. Drechsler, J. Preussner, In situ growth of catalytic active Au−Pt bimetallic nanorods in thermoresponsive core−shell microgels, ACS Nano 4 (12) (2010) 7078–7086, https://doi.org/10.1021/nn102622d.
[27] H. Yuan, C.G. Khoury, H. Hwang, C.M. Wilson, G.A. Grant, T. Vo-Dinh, Gold nanostars: surfactant-free synthesis, 3D modelling, and two-photon photoluminescence imaging, Nanotechnology. 23 (7) (2012) 075102, https://doi.org/10.1088/0957-4484/23/7/075102.
[28] G.R.C. Rodríguez, G.H. Gauthier, L.O. Ladeira, J.A.S. Cala, D.L. Cataño, Effect of pH and chloroauric acid concentration on the geometry of gold nanoparticles obtained by photochemical synthesis, J. Phys. Conf. Ser. 935 (2017) 012027, https://doi.org/10.1088/1742-6596/935/1/012027.
[29] K. Park, L.F. Drummy, R.C. Wadams, H. Koerner, D. Nepal, L. Fabris, R.A. Vaia, Growth mechanism of gold nanorods, Chem. Mater. 25 (4) (2013) 555–563, https://doi.org/10.1021/cm303659q.
[30] M. Grzelczak, J. Pérez-Juste, P. Mulvaney, L.M. Liz-Marzán, Shape control in gold nanoparticle synthesis, Chem. Soc. Rev. 37 (2008) 1783–1791, https://doi.org/10.1039/b711490g.
[31] C.M. Hessel, V.P. Pattani, M. Rasch, M.G. Panthani, B. Koo, J.W. Tunnell, B. A. Korgel, Copper selenide nanocrystals for photothermal therapy, Nano Lett. 11 (6) (2011) 2560–2566, https://doi.org/10.1021/nl201400z.
[32] Y. Liu, K. Ai, J. Liu, M.o. Deng, Y. He, L. Lu, Dopamine-melanin colloidal nanospheres: an efficient near-infrared photothermal therapeutic agent for in vivo cancer therapy, Adv. Mater. 25 (9) (2013) 1353–1359, https://doi.org/10.1002/adma.201204683.
[33] C. Biglione, E.A. Glitscher, S. Arora, B. Klemke, M. Giulbudagian, P. Laux, A. Luch, J. Bergueiro, M. Calderón, Galvanic replacement as a synthetic tool for the construction of anisotropic magnetoplasmonic nanocomposites with synergistic phototransducing and magnetic properties, ACS Appl. Mater. Inter. 12 (51) (2020) 56839–56849, https://doi.org/10.1021/acsami.0c18096.